Modelling and Experimental Investigations on Degradation of Microcomponents in Power Cycling

M. Thoben, W. Staiger, DaimlerChrysler Research and Technology, LAB 14, Frankfurt, Germany;
J. Wilde, IMTEK, University of Freiburg, Germany

Abstract
Thermomechanical damage is one of the principal failure causes of microcomponents and microsystems. Often the basic defect mechanisms are crack initiation and subsequent crack propagation in interfaces or materials. The fatigue behavior of microcomponents can in many cases be described by the Manson-Coffin-Formula. This model is well-suited for comparison of different designs relative to each other but it will fail when a realistic lifetime prognosis is expected. Therefore we worked out a concept which is based on the computation of the strain range distribution in the interconnection by finite elements simulations and subsequent calculation of the cyclic crack propagation rate. Using this method in combination with calibration measurements it is possible to predict the lifetime of electronic assemblies with significantly improved precision compared to the Low-Cycle-Fatigue approaches.

1. Introduction

The use of electrotraction in cars is restricted among other factors by the high price of such vehicles. One of the cost sources is the electronic power converter device which mainly consists of three transistor/diode half-bridges. In addition to the semiconductor modules, an inverter comprises a cooling system, Fig. 1, and the control part of the electronics. With new generations of IGBT (Insulated Gate Bipolar Transistor) power modules, great progress has been made in recent years on the components level. Such modules have been applied mainly in industrial motor drive applications. The use of standard IGBT modules limits the possibilities for optimization with respect to costs, thermal performance and reliability. Hence for large production volumes, an integrated customer specific design appears to be very promising. In this paper we therefore present a methodology and results of such an systematic design approach which can be utilized in the development of power converters for electrovehicles.

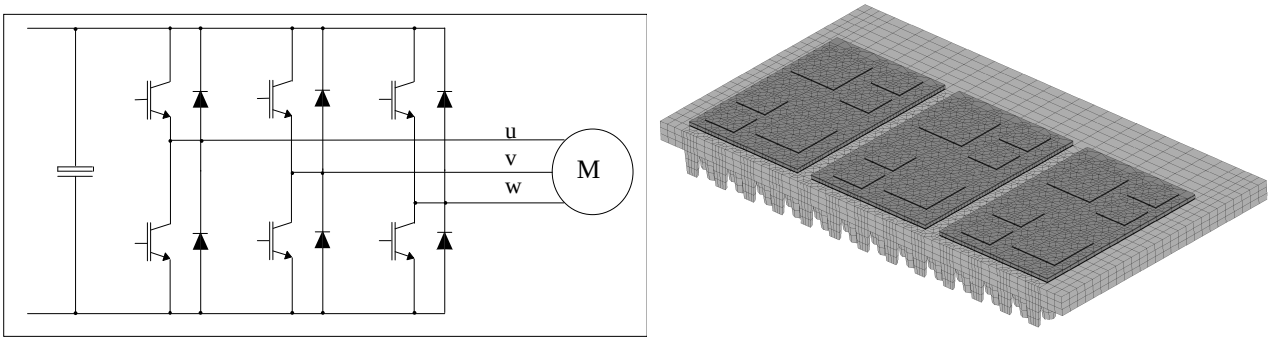

Fig. 1: Circuit diagram of a DC/AC power converter and CAD/FE model including the heat sink.

2. Specifications and Aim of the Optimization

The specifications for an intelligent, integrated inverter and the electronic architecture were derived from the requirements for the traction system of the car, Table 1:

Traction Power:	40 kW peak, 20 - 30 kW continuous
Design:	water cooled heat sink, 6 or 9 DCB substrates
Semiconductors:	IGBT: 600 V, 200 A, 2 per substrate
	diodes: 600 V, 100 or 200 A, 4 or 2 per substrate
Reliability:	T_{max}<125 °C in semiconductors
	>500 temperature cycles, -40 to +85 °C
	>30,000 power cycles, +65 to 125 °C

Table 1: Specification for a power inverter for automotive electrotraction.

The concept of the converter module was a result of an initial design study, Fig. 1. The unit mainly consists of a water cooled heat sink, the power module with three half-bridges and the driving circuitry, not shown here. Design variables comprised number, size and type of half bridges, geometry of the heat sink, attachment method of the modules to the heat sink and materials for assembly, packaging and substrates. The employed design-for-reliability concept makes it possible to optimize power converters under aspects of thermal management, mechanical behavior and soldered joint reliability:
The circuit diagram and a first layout is created on the basis of engineering experience. This design is subjected to thermal management simulations using also Computational Fluid Dynamics (CFD) analyses to supply boundary conditions. The thermal analysis itself supplies an input for the Finite Elements Method (FEM)-simulation of the thermomechanical behavior of the power modules.

3. Thermal Management

The principal questions in this part of the investigation are the attachment method of the modules to the heat sink and the heat sink design itself. A heat exchanger's performance is described in terms of the effective heat transfer coefficient h_{eff}, which defines the heat that is transferred over the base area into the medium with a unit temperature difference. In the case of parallel straight cooling channels h_{eff} lies in the order of 6,000 W/m^{2}K. More efficient designs are characterized by many discrete fins protruding into the medium with h_{eff} in the order of 13,000 to 15,000 W/m^{2}K. Evidently, the heat sink material itself also affects the efficiency of the heat transfer, Table 2. These values of h_{eff} are used as boundary conditions for subsequent thermal management calculations.
The values of the dissipated power over time are inputs from electrical simulations determined for realistic driving conditions of the electrovehicle. The critical state is acceleration at a slope with values of dissipated power as follows: IGBT: 380 Watt peak, 110 W average, diodes: 80 Watt peak, 23 W average, and for the total module an average of 1880 W.

Semiconductors	Substrate Material	Heat Sink Material	h_{eff} [W/m^{2}K]	T [°C] IGBT	T [°C] Diode	Type of assembly
Manuf. 1	HP DCB	Al+TMC	15,000	138	138	standard modules
Manuf. 1	HP DCB	LC steel	13,000	131	132	integrated
Manuf. 1	HP DCB	Al+Cu	15,000	131	133	standard modules
Manuf. 1	HP DCB	TMC	15,000	117	119	integrated
Manuf. 1	LP DCB	TMC	15,000	129	127	integrated
Manuf. 2	HP DCB	TMC	15,000	129	112	integrated

Table 2: Maximum peak temperatures as a results of thermal simulations for different types of substrate and heat sink materials.

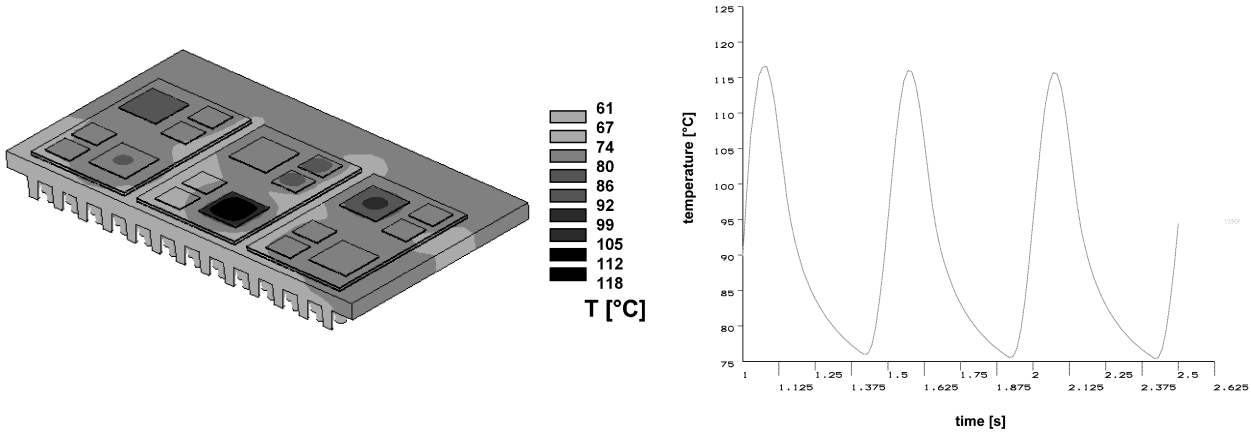

Fig. 2: Left: typical temperature distribution of a half bridge module during operation with a motor frequency of 2 Hz. Right: transient temperatures.

Table 2 demonstrates that the evaluation of several alternatives significantly reduces the number of design options. Possible heat sink materials are copper, low-carbon (LC) steel, and a thermomechanically matched composite material (TMC). For the substrates high and low performance Direct Bonded Copper (HP DCB) and (LP DCB) were considered. In transient simulations the temperatures of the IGBTs exceed those of the diodes, Fig. 2. Based on this study only such designs can be considered as efficient which exhibit only one integrated mounting plate which also serves as a heat sink. Furthermore only high performance ceramic substrates (HP DCB) will yield relatively low transient temperatures in the semiconductors and consequently will avoid potential reliability hazards.

4. Thermomechanical Management

4.1 Materials

Material	Thermal Coefficient of Expansion α in 10^{-6}/K	Young's Modulus E in MPa (T in °C)
LC steel	12.5	207,000
Copper	17.0	125,000
Aluminum	20.0 to 25.0	69,700
TMC	7.2	226,000
Pb92 Sn Ag2	22.0 to 27.5	24,100 - 28 T
Sn62 Pb Ag2	25.0	33,200 –173 T
Silicon (100)	2.1 to 3.2	131,000
LP DCB	4.4 to 7.2	276,000
HP DCB	3.7	310,000

Table 3: Thermomechanical properties of assembly materials from [2] and suppliers' data.

For the integrated designs with direct heat sink attachment, the principal options for improvement are the materials of the heat sink and the substrate, Table 2. Fabrication restricts the solder materials to Pb92.5 Sn5 Ag2.5 for the chip attachment and to Sn62 Pb36 Ag2 for the substrate bonds. Both solders show characteristic non-linear stress-strain behavior (plasticity), Fig. 3. Moreover, due to

the high homologous temperatures in operation, both materials tend to creep, i. e. to deform continuously under mechanical stress. The creep rate dε/dt is sensitive to variations of stress level and temperature, Fig. 3. It is indispensable to take into account both mechanisms in a realistic thermomechanical lifetime assessment. The results of mechanical tests have been fitted to a so-called viscoplastic deformation law, combining plasticity and creep in an unified physical model [1]. A kinetic equation defines a dependency between viscoplastic strain rate $d\varepsilon_v/dt$, stress σ and temperature T.

$$\dot{\varepsilon}_{\mathrm{v}} = A \cdot e^{-\frac{Q}{RT}} \left[\sinh(\xi \cdot \frac{\sigma}{s}) \right]^{\frac{1}{m}} \qquad (1)$$

The variable s takes into account the materials thermomechanical history, like strain hardening and strain softening. Hence a second set of equations defines the evolution of $\dot{s}$. a, B, h_o, A, Q, $\hat{s}$ and m are materials constants [1].

$$\dot{s} = \left\{ h_0 (|B|)^a \cdot \frac{B}{|B|} \right\} \cdot \dot{\varepsilon}_{\mathrm{v}} \; ; a > 1 \qquad \mathrm{B} = (1 - \frac{\mathrm{s}}{\mathrm{s}^*}) \qquad s^* = \hat{s} \cdot \left[\frac{\dot{\varepsilon}_{\mathrm{v}}}{A} e^{\frac{Q}{RT}} \right]^n \qquad (2, 3, 4)$$

The parameters of this model were implemented into the FEM software tool.

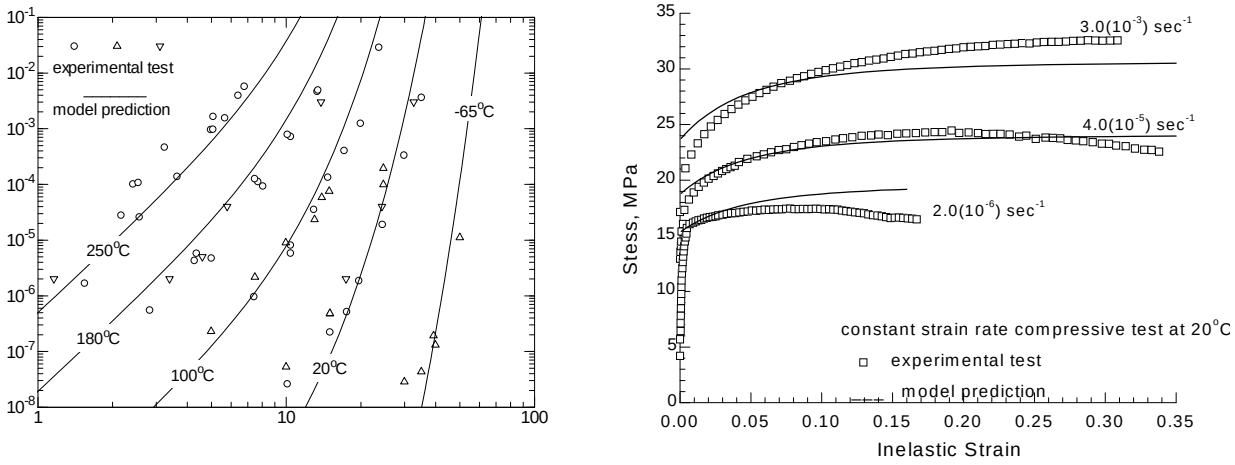

Fig. 3: Plastic deformation and creep properties of the solder alloy Pb92.5 Sn5 Ag2.5: measured data and multi-variant regression curves to a viscoplastic model.

4.2 Finite Element Models

Due to the complexity of even a single half-bridge assembly, very large finite-element models will be required for three-dimensional simulations. As the simulations have to be performed with non-linear and time-dependent materials properties, long computational times are to be expected on typical workstations in the design environment. Consequently the thermomechanical analysis was first reduced from three-dimensional models to two-dimensional ones. Comparative investigations showed that for the given geometry such a simplification will not lead to prohibitive errors.

In a first step, critical sections were identified on the module by 3D linear analysis, Fig. 4. These represent the planes of investigation for the 2D-FEM simulations, which lie parallel to the diagonal axes of the IGBT chip and the substrate respectively. For those sections the meniscus shapes of the soldered joints were modeled, Fig. 4. Metallographic studies showed that the soldering process can yield a range of geometry of the solder gap with a typical thickness of the solder layer between 50 and 100 μm. Consequently, the effect of gap width also has to be considered in the design.

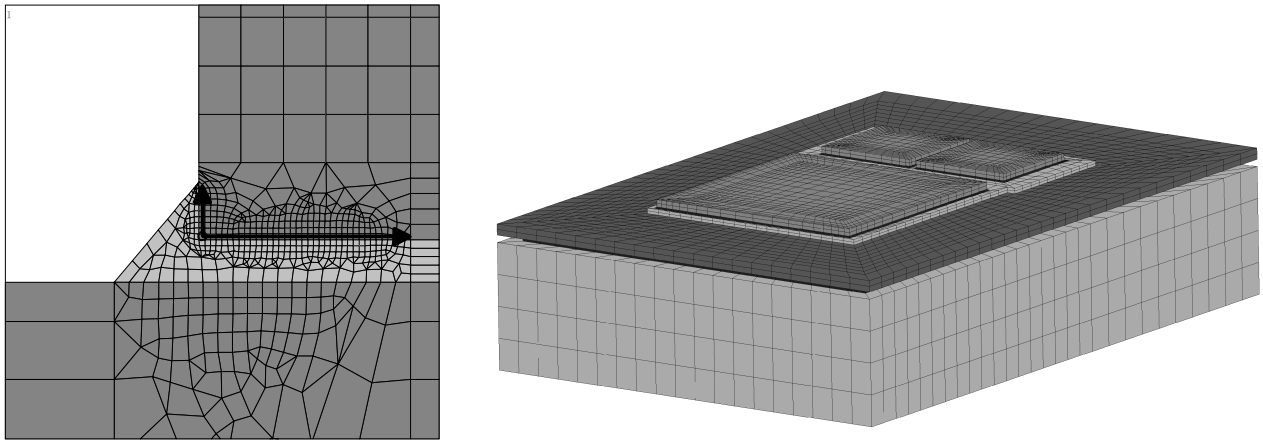

Fig. 4: 2D an 3D Finite Elements models of a half-bridge power module. These include substrate/ heat sink attachment and the solder material.

4.3 Temperature Cycles

In accordance with the physical lifetime tests to be performed in the qualification phase, the following load cycles were defined:

Temperature Cycle:	-40 to 85 °C / 85 min	passive cycle in a temperature chamber
Power Cycle:	+45 to 125 °C / 15 min	active heating cycle by dissipated power

For the passive cycle, temperature conditions are directly applied to the model. For the active cycle the temperature distribution of thermal 3D models were transferred to the mechanical 2D models within the FEM software package.

4.4 Results of the FEM simulations

The finite element analysis provides us with data about the distribution of stresses and strains in the assembly and especially in the soldered joints. These are dependent of position, space direction and time. Evidently, maximum values occur near the solder joint menisci and especially on edges, corners or materials transitions. The locations of extreme values are very similar for solder joints with different geometries, Fig. 5. Also the critical points, i. e. nodes and elements, are the same at high and at low temperatures.

Time-dependent stresses and strains at critical nodes or elements are extracted from the FEM results files. A plot of stress versus strain will provide hysteresis loops which define the cyclic deformation of the soldered joints. All four stress and strain components σ_x, σ_y, σ_z, σ_{xy} and ε_x, ε_y, ε_z, ε_{xy} have to be taken into account, Fig. 6. From the hysteresis loops the equivalent values of stresses, strains and strain amplitudes, $\Delta\varepsilon_v$, are computed in accordance with the von Mises formulas and ASME code. This procedure was applied for the data of the substrate/heat-sink attachments as well as for the substrate soldered joints.

The lifetime of the soldered joints is defined by the number of cycles N at which a certain failure criterion is reached. Ideally this would be an electrical failure, but it is difficult to derive electrical criteria from mechanical simulations. Consequently the Coffin-Manson-Model has been frequently used as a replacement for a functional failure criterion in the lifetime prediction of soldered joints. In this case it is assumed that the thermal cycles will induce low-cycle fatigue mechanisms in the soldered bonds which will be damaged in two subsequent steps:

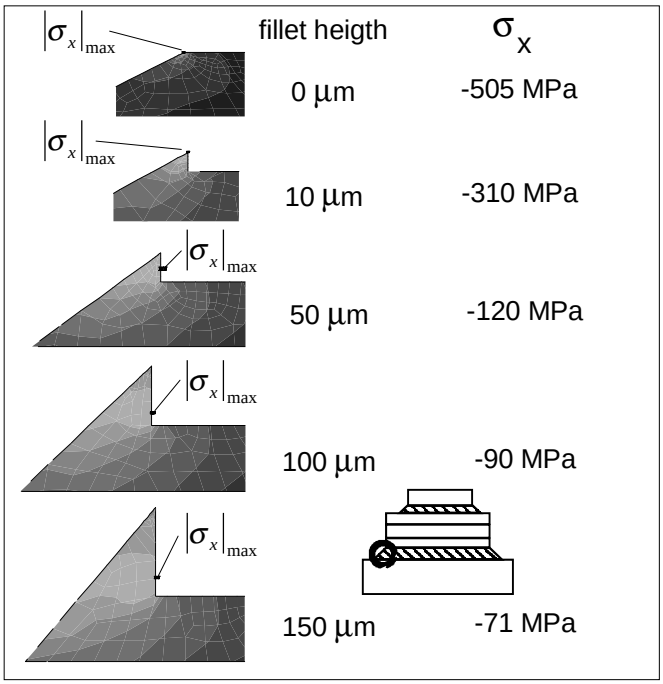

Fig. 5: Distribution of stresses in solder joints between substrate and heat sink: linear elastic study of meniscus geometry.

4.5 Crack Formation

First a small crack will be formed at locations where high strain amplitudes occur. Such critical regions frequently lie near surfaces or interfaces of the soldered joint. The number of cycles to crack initiation N_a will be a function of the material constants C and K and of the viscoplastic strain amplitude $\Delta\varepsilon_v$:

$$N_a = K \cdot \left(\frac{\Delta\varepsilon_v}{2} \right)^{1/C} \qquad (5)$$

with K = 1.84 and 1/C=-1.05 in the case of Pb92.5 Sn Ag2.5 and a load drop of 10 % [3, 4].
According to our investigation the soldered joints of the IGBT to the DCB substrate tend to exhibit much higher strain amplitudes than those of the substrate to the heat exchanger. Hence the latter ones will tolerate much more cycles until a crack is formed. Consequently the analysis was focussed on the IGBT/DCB substrate bonds.

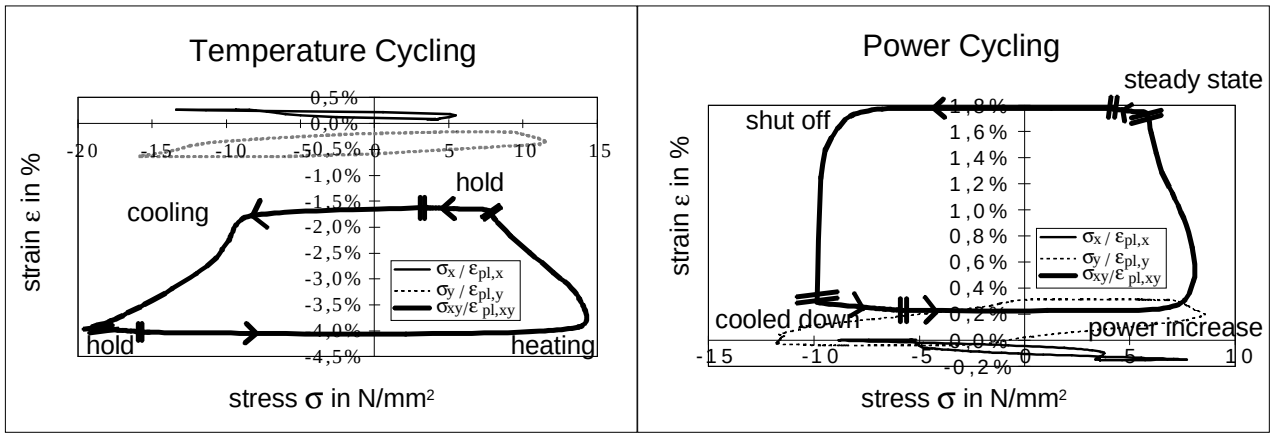

Fig. 6: Stress-strain hysteresis loops in the critical area of an IGBT/substrate sink soldered joint.

- Assemblies with HP DCB generally tolerate significantly more cycles than those with LP DCB as they exhibit a better thermomechanical match to the silicon, Table 4.
- Already after 1500 to 2000 cycles first cracks must be expected near the chips' corners.
- The heat sink material will not affect the reliability of the IGBT chips' solder joints.
- An increase of the solder gap width will slightly increase the number of cycles to crack start.

So it was possible to select one design as the comparably best one under aspects of cooling capability and reliability: It is the one with substrates made of high performance (HP) DCB and a heat sink consisting of a thermomechanically matched composite (TMC). Unfortunately in view of our experimental work the values of cycles to crack start do not correspond very well with failure data. Consequently a method was developed to estimate the number of cycles to failure more precisely:

4.6 Crack Propagation

After a crack has been formed, it tends to grow under the effect of cyclic strains. The kinetics of this process are described adequately in terms of strain amplitude $\Delta\varepsilon_v$ and materials parameters. The following formula was derived by a fit of experimental data from [3, 4] to a model published by [5]:

$$\frac{da}{dN} = 0.305 * \Delta\varepsilon_v^{1.326} \qquad (6)$$

The numbers of cycles N_i to an actual crack length a can then be determined by a numerical integration when the dependency of $\Delta\varepsilon_v$ on the position x across the soldered joint is available as a result of the FEM simulation.

$$N_i = \int_0^a \frac{dN}{da}\,dx = \int_0^a \frac{1}{0.305 * \Delta\varepsilon_v^{1.326}}\,dx \qquad (7)$$

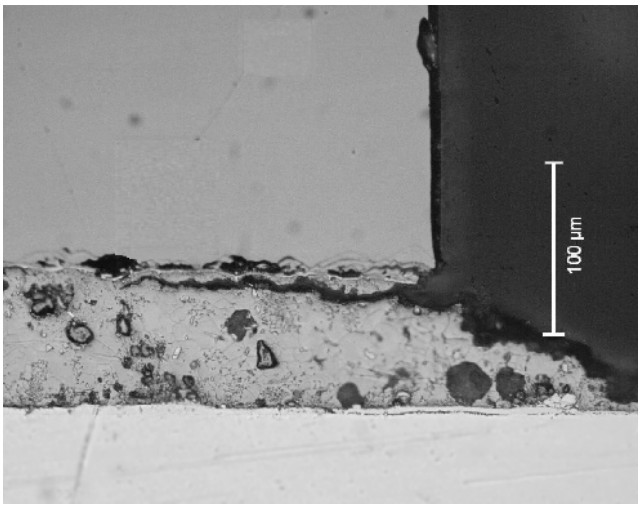

Fig. 7: Metallographic cross section of the IGBT solder joint in a power module after approximately 38,000 power cycles.

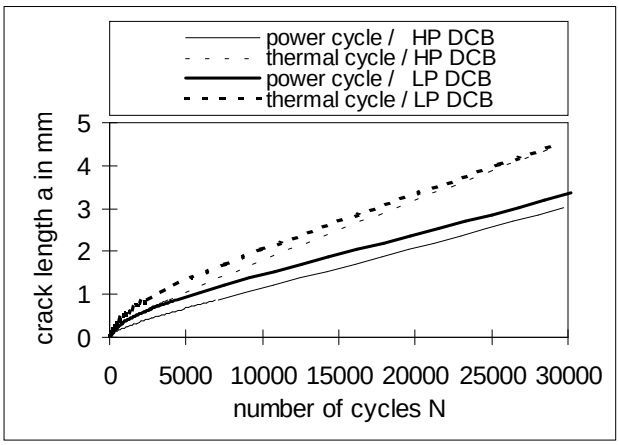

Fig. 8: Simulated crack length as a function of the number of cycles in the IGBT solder joints.

Based on these formulas and on the results of the FEM, the evolution of crack length with the number of cycles was computed. The crack length increases slower in the case of power cycles compared to thermal cycles, Fig. 8, mainly due to the higher temperature amplitude of the passive cycles compared to the active cycle. Designs with HP DCB are superior to those with LP DCB as the

crack length grows somewhat slower with increasing number of cycles. Cracks are expected to start in the solder material below the corners of the chips due to concentrations of strain amplitude. For the given IGBT chip sizes a crack length of a = 2 mm will already have a measurable effect on the thermal resistance and therefore will probably accelerate the failure process significantly. Typically in our case 2 mm cracks have to be expected after 17,000 to 22,000 cycles. In reliability tests, however, after approximately 38,000 power cycles cracks could be detected in the soldered joints of the IGBT semiconductors on the DCB substrates, Fig. 7. These cracks are found precisely in the regions of maximum stresses and strains.

Model No.	Heat Sink Material	Substrate Material	Solder Gap Width	Cycles to Crack Start	Cycles to a Crack of 2 mm
A	TMC	HP DCB	70 µm	1514	21,051
B	LC steel	HP DCB	50 µm	1680	22,235
C	LC steel	HP DCB	70 µm	1753	22,364
D	LC steel	HP DCB	90 µm	1770	22,361
E	Cu	HP DCB	70 µm	1965	21,410
F	TMC	LP DCB	70 µm	484	16,636
G	LC steel	LP DCB	70 µm	488	17,130

Table 4: Results of lifetime simulation of IGBT solder joints in power cycles.

5. Conclusions

Substantial benefits can be earned in the design of power inverter for automotive traction by use of a systematic design-for-reliability procedure. To that purpose it is necessary to link the engineering teams as well as the software tools in the fields of electrical design, circuit layout, mechanical CAD, computational fluid dynamics, thermal management and reliability prognosis. In such manner an optimization of the module with respect to thermal behavior, reliability, manufacturability and costs is possible in order to meet technical and economical specifications. Also design processes are accelerated significantly as the effort and time for prototyping and testing is reduced. Up to now it was only possible to design power converters which were optimized in comparison to other competing designs. The concept of this work takes into account also the effect of crack propagation in soldered joints which offers the possibility for a more realistic but still conservative lifetime prediction. The precision of the simulations can still be improved by calibration tests.

6. References

[1] Brown, S. B., K. H. Kim and L. Anand, Int. Journal of Plasticity 5, 1989, pp. 95 - 130.

[2] Püttner, H., A. Rukwied and J. Wilde: “Lifetime properties of the solder material Sn62PbAg2 (in German)“, Proc. 1st European Conf. on Electronic Packaging Technology 1994. Deutscher Verlag fuer Schweisstechnik, Duesseldorf, 1994, pp. 150 - 153.

[3] Solomon, H. D., “High and low temperature strain life of a Pb rich solder“, J. Electronic Packaging, June 1990, pp. 123 - 128.

[4] Solomon, H. D., “Predicting thermal and mechanical fatigue lifes from isothermal low-cycle data“, in *Solder Joint Reliability*, Ed.: J. H. Lau, Van Nostrand Reinhold, New York, 1991.

[5] Darveaux, R., “Crack initiation and growth in surface mount solder joints“, Proceedings ISHM ‘93. International Society for Hybrids Microelectronics, pp. 86 - 97.